Ceramics International 48 (2022) 3236–3242

Contents lists available at ScienceDirect

Ceramics International

journal homepage: www.elsevier.com/locate/ceramint

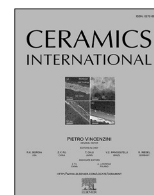

Y-doped HfO_2 deposited by atomic layer deposition using a cocktail precursor for DRAM capacitor dielectric application

Jenam Kim [a], Byung Seok Kim [a], Ae Jin Lee [a], Dong Hee Han [a], Ji Hyeon Hwang [a,b], Youngjin Kim [b], Ki-Chang Song [c], Hansol Oh [c], Sangho Kim [c], Yongjoo Park [c,**], Woojin Jeon [a,*]

[a] *Department of Advanced Materials Engineering for Information and Electronics, And Integrated Education Program for Frontier Science & Technology (BK21 Four), Kyung Hee University, Yongin, Gyeonggi, 17104, South Korea*

[b] *Soft Hybrid Materials Research Center, Korea Institute of Science and Technology, Seoul, 02792, South Korea*

[c] *Advanced Research Development Team, SK Trichem Co. Ltd., Sejong, 30068, South Korea*

ARTICLE INFO

Keywords:
Hafnium oxide
Yttrium oxide
Cocktail precursor
Atomic layer deposition
Insulator
Oxygen vacancy
Phase transformation
Dopant

ABSTRACT

A Y-doped HfO_2 thin film deposited using a cocktail precursor for a DRAM capacitor dielectric application was investigated. It has been difficult to adapt HfO_2, a potential high-dielectric-constant material, deposited by a typical thin-film deposition technique to actual devices owing to its low dielectric constant of approximately 20, resulting from its monoclinic-phase crystal structure. Although several methods have been investigated to increase the dielectric constant by crystal structure transformation to the tetragonal phase, which has a dielectric constant as high as approximately 40, the formation of the monoclinic phase was not successfully suppressed. In this study, the tetragonal-phase formation of HfO_2 thin films was investigated using a cocktail precursor consisting of Y and Hf precursors. The monoclinic formation suppression mechanism in the Y-doped HfO_2 thin film was determined from the physical and chemical analyses results. Moreover, the leakage current change caused by the introduced oxygen vacancy with respect to the Y dopant concentration was investigated. Improved electrical properties of the dielectric constant and leakage current were achieved with Y-doped HfO_2.

1. Introduction

HfO_2 has attracted considerable attention as a representative high-dielectric-constant (*k*) material for gate dielectric [1–5] and capacitor dielectric applications [6–8]. To make HfO_2 a suitable high-*k* material, numerous studies on achieving higher *k* values by inducing tetragonal-phase crystallisation have been conducted [4,5,9–16]. Employing dopants, such as Al_2O_3 [5,9–11] or carbon [12], which can induce distortion in the lattice, results in HfO_2 tetragonal-phase formation. The template effect from the insertion layer was introduced [14,16]. However, increasing the *k* value using the above methods inevitably leads to degradation in the leakage current [17]. Moreover, these methods cannot totally suppress the formation of the monoclinic phase. This originates from the energy-level difference between the monoclinic and tetragonal phases [18–20]. HfO_2 has many possible crystal structures: monoclinic, tetragonal, cubic, and orthorhombic. The most stable crystal structure is determined based on the conditions. Generally, a thin film with a thickness of less than approximately 3 nm tends to have the tetragonal phase, and one with a thickness of more than approximately 3 nm tends to have the monoclinic phase. This is because the monoclinic phase has lower bulk energy and higher surface energy than the tetragonal phase. This thickness boundary of monoclinic and tetragonal-phase transition is called the ‘critical thickness’ [21]. While the ZrO_2 thin film tends to have a tetragonal crystal structure with a thickness of tens of nanometres [11,22], the HfO_2 thin film generally has a monoclinic crystal structure [11]. This is because of the different critical thicknesses of 3 and 15 nm for HfO_2 and ZrO_2, respectively [21], resulting in that the HfO_2 thin film generally has monoclinic phased crystal structure, in contrast to that the ZrO_2 thin film has tetragonal/cubic phase even in using the precursor with same ligand chemistry and employing same process conditions. Consequently, the aforementioned methods, which only induce local lattice distortion at the interface, cannot achieve full transformation to the tetragonal phase. Therefore, a method for stabilising the tetragonal phase in the whole bulk level of HfO_2 thin film is required to achieve a fully crystallised HfO_2 thin film with a tetragonal phase.

* Corresponding author.
** Corresponding author.
E-mail addresses: yj.park81@sk.com (Y. Park), woojin.jeon@khu.ac.kr (W. Jeon).

https://doi.org/10.1016/j.ceramint.2021.10.097
Received 13 August 2021; Received in revised form 14 October 2021; Accepted 18 October 2021
Available online 30 October 2021
0272-8842/© 2021 Elsevier Ltd and Techna Group S.r.l. All rights reserved.

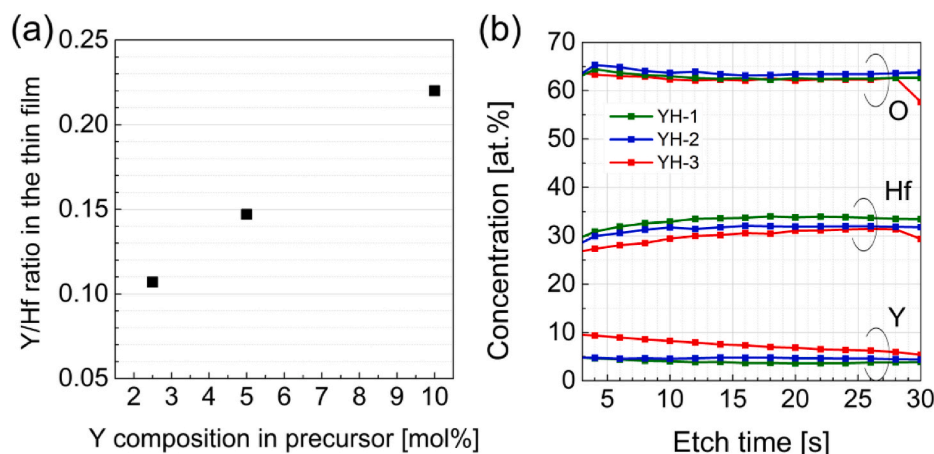

Fig. 1. (a) Y/Hf ratio in the deposited thin films and (b) depth profiles for O, Hf, and Y of the YH-1, YH-2, and YH-3 thin films, respectively.

In the ZrO_2 thin-film case, a solution for stabilising the tetragonal phase from the bulk level has already been reported: yttrium-stabilised zirconia (YSZ) [23–25]. The monoclinic phase is the most stable crystal structure in bulk ZrO_2 films. This is because the ionic radius of Zr^{4+} is too small to stabilise the tetragonal structure, with a coordination number of eight. When tetravalent Zr^{4+} is replaced by trivalent Y^{3+}, a charge imbalance is induced, resulting in the retention of a coordination number of eight, and a higher fraction of Zr atoms can adopt a coordination number of seven. Consequently, the tetragonal phase is stabilised and the transformation to the monoclinic phase is suppressed. The calculation result predicted that 12.5 mol% of Y stabiliser in ZrO_2 must be added to reduce the coordination number of all cations to seven [26–28], where the tetragonal phase would be stabilised and transformation to the monoclinic phase would be suppressed. HfO_2 is known to have quite similar physical properties and crystallisation behaviours to those of ZrO_2. Hence, Y doping would be an effective solution to obtain the tetragonal phase in a thin film with a thickness greater than the critical thickness. Accordingly, achieving homogeneous doping of Y in the entire range of HfO_2 thin films is important for implementing the tetragonal phase.

In the general atomic layer deposition (ALD) process, doping of a dopant in a thin film is carried out by a constitution of a supercycle with ALD subcycles of the dopant and thin film [11,29,30]. However, the dopant profile obtained by this layer-by-layer doping method using the ALD supercycle inevitably has a locally concentrated gradient [17,31,32]. Consequently, the property enhancement deliberated by introducing the dopant was not effectively achieved [33–36]. In contrast, the cocktail precursor can achieve a homogeneous dopant concentration in the deposited thin film. Therefore, in this study, a cocktail precursor of Y and Hf precursors was employed for ALD.

2. Experimental procedure

HfO_2 thin films were deposited by means of ALD (iOV dX1, iSAC research) using $HfCp(NMe_2)_3$ and O_3 as the Hf precursor and oxygen source, respectively. The substrate consisted of 100-nm TiN as a bottom electrode on a thermally oxidised (100) Si wafer. The Hf precursor was introduced into the process chamber with Ar carrier gas using a bubbler system. For the deposition of Y_2O_3-doped HfO_2 (Y-HfO_2) thin films, a cocktail precursor consisting of $HfCp(NMe_2)_3$ and a cyclopentadienyl yttrium amide (SK Trichem Co., Ltd.) as the Hf and Y precursors, respectively, was employed. The precursor was kept on room temperature. The vaporizer was heated to 150 °C to vaporize the liquid cocktail precursor injected 0.05 g/m controlled by liquid mass flow controller with Ar flow of 100 sccm as a carrier gas. The ALD sequence was consisted of precursor feeding, Ar purge, ozone feeding, and Ar purge of 5, 30, 5, and 10 s, respectively. The growth per cycle (GPC) in the saturation ALD condition was 0.106 nm/cycle regardless to the Y concentration of the cocktail precursor. The ALD sequence was conducted 104 cycles to deposit 11-nm-thick Y-HfO_2 thin film. In addition, 11-nm-thick Y-HfO_2 thin films were deposited using the cocktail precursor with various Y concentrations to vary the composition of Y in the Y-HfO_2 thin film. The Y-HfO_2 thin films with varying Y compositions are denoted as YH-1, YH-2, and YH-3. To ensure a consistent vapour pressure ratio of Y and Hf precursors during the process, a liquid delivery system was utilised. A mixture of Y and Hf precursors with the same concentration as that of the cocktail precursor was injected into the process chamber during the precursor feeding step. The process temperature was maintained at 300 °C. Postdeposition annealing was performed at 600 °C for 30 s under N_2 ambient conditions to crystallize the thin films. To measure the electrical properties, a metal–insulator–metal (MIM) capacitor was fabricated with a top electrode, which consisted of 50-nm-thick Ti and 50-nm-thick Pt films that were defined by a metal shadow mask with a 300-μm-diameter hole.

The thickness of the insulator films was measured by a spectroscopic ellipsometer (ESM-300, J. A. Woollam). The depth profiles of the composition and chemical status of the thin films were analysed using X-ray photoelectron spectroscopy (XPS, K-Alpha+, Thermo Fisher Scientific). Glancing angle incident X-ray diffraction (XRD, X'pert Pro, PANalytical) was used to examine the crystal structure of the films with an incident angle of 0.5°. The electrical properties were evaluated by measuring the capacitance–voltage and the current–voltage characteristics using Agilent 4284 and 4155C, respectively.

3. Results and discussion

The composition of the thin film was investigated through XPS analyses (Fig. 1). From the atomic concentration values of Y and Hf measured at an etching time of 20 s, as shown in Fig. 1(a), the Y/Hf ratios of the YH-1, YH-2, and YH-3 films were calculated to be 0.107, 0.147, and 0.220, respectively. The depth profile analysis revealed that all the Y-HfO_2 thin films had a homogeneous composition of O, Hf, and Y in the depth direction, as shown in Fig. 1(b). In the YH-1 and YH-2 thin films, the Y concentration in the thin film was almost identical at all examined points. In the case of the YH-3 thin film, the Y concentration linearly increased to the surface. Although a concentration gradient was observed, there was no fluctuation of concentration in the depth direction, which is generally observed in a thin film doped with a dopant by executing the ALD supercycle process [17,31]. When the doping is separately conducted by employing the dopant ALD subcycle process for thin-film deposition, i.e., the Al_2O_3 subcycle for Al doping of the TiO_2 thin film, the dopant concentration profile has a large gradient with a

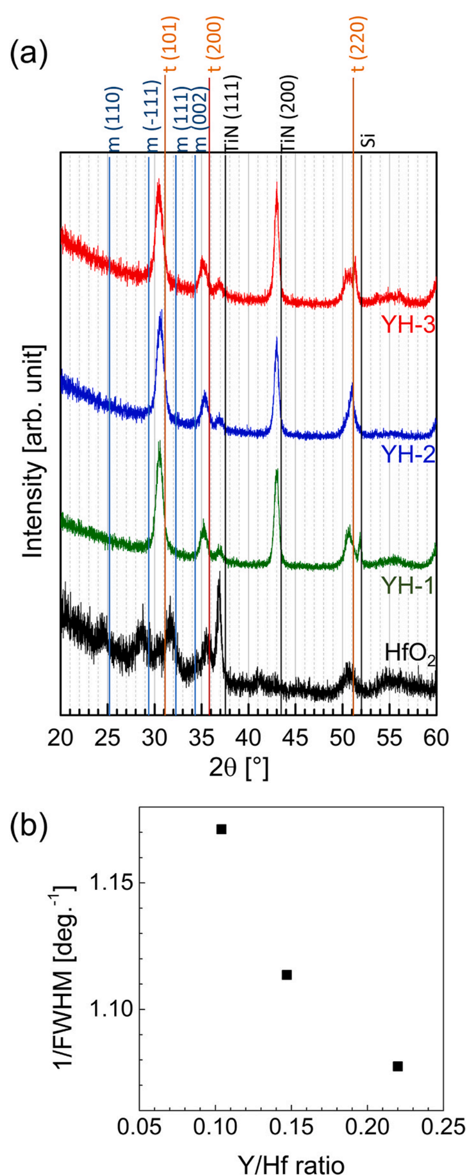

Fig. 2. (a) XRD patterns of HfO2, YH-1, YH-2, and YH-3 thin films and (b) Y/Hf ratio versus the grain size (calculated from the reciprocal value of FWHM of the t(101) peak from the XRD pattern in Fig. 2(a)).

peak where the subcycle is executed [32]. In other words, a homogeneous dopant concentration profile cannot be achieved through doping by employing the ALD supercycle process. However, a homogeneous Y concentration profile was obtained by employing the cocktail precursor because the dopant and thin film were deposited simultaneously. Therefore, the Y-HfO_2 thin-film deposition process with a homogeneous dopant concentration profile was successfully achieved by adopting the cocktail precursor.

The crystal structure of the Y-HfO_2 thin films was investigated using XRD measurements. The XRD spectra of pristine HfO_2 and Y-HfO_2 with various Y/Hf ratios are shown in Fig. 2(a). In the case of the HfO_2 thin film, the XRD spectrum indicates that the HfO_2 thin film has mixed crystallinity with monoclinic and tetragonal phases. As determined from the relative peak intensity, the major crystal structure was in the monoclinic phase, agreeing with previous results that HfO_2 thin film deposited by ALD generally has a monoclinic-phase crystal structure [11,37]. In contrast to the pristine HfO_2 thin film, the Y-HfO_2 thin films were solely composed of the tetragonal phase, and no contribution of the monoclinic phase was observed in the XRD spectra. In a previous study

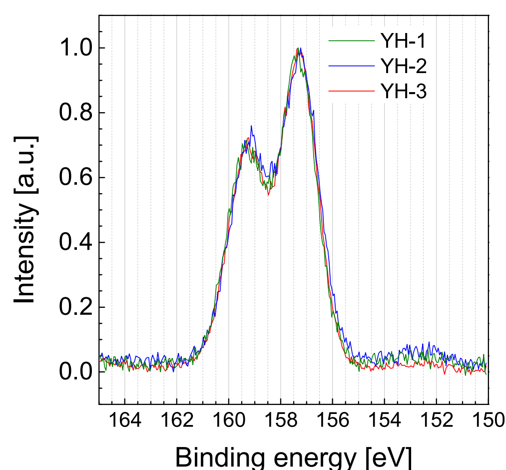

Fig. 3. Y 3d XPS profiles of YH-1, YH-2, and YH-3 thin films.

on the induction of tetragonal-phase crystallisation by adopting a dopant, such as Al_2O_3, it was impossible to completely eliminate the contribution of the monoclinic phase in the crystal structure of the HfO_2 thin film [11,38]. Moreover, there is a certain upper limit on increasing the dopant concentration because too high a dopant concentration induces amorphisation rather than tetragonal-phase crystallisation [11]. It is believed that this limitation of tetragonal-phase transformation by employing the dopants originates from the phase transformation mechanism that induces stress at the surface of the HfO_2 grain, not from the bulk region. The effect, which induced tetragonal-phase formation using a dopant in previous cases, was confined only to the localised region near the surface of the thin film or the grain; hence, the monoclinic phase still should remain in the bulk region. When the dopant concentration is too high, it is incorporated into the bulk, resulting in the suppression of crystallisation and, in turn, amorphisation. Consequently, the dopants previously examined cannot prevent the formation of the monoclinic phase. However, Y doping by introducing Y_2O_3 into the HfO_2 thin film by adopting the cocktail precursor exhibited full transformation to the tetragonal phase in all the examined Y concentrations. This crystallisation behaviour agreed well with the previous results for YSZ [39]. As the Y dopant in the ZrO_2 thin-film-induced tetragonal--phase crystallisation, an oxygen vacancy (V_O) introduced by the stoichiometry difference between Y_2O_3 and HfO_2 formed in the HfO_2 thin film, resulting in the formation of a tetragonal phase. Because Zr^{4+} and Hf^{4+} have almost identical ionic radii, the same mechanism would affect the formation of the tetragonal phase in the HfO_2 thin film by doping with Y.

The most distinctive difference between Y and the previously reported dopants is the origin of the tetragonal-phase transformation. In contrast to previous dopants, Y induces a tetragonal-phase transformation from the bulk of the HfO_2 grain. Therefore, the Y dopant can achieve tetragonal-phase formation in the entire region of the HfO_2 thin film. Furthermore, the grain size of the HfO_2 thin film affected the formation of the tetragonal phase. The critical thickness is governed by the formation energy difference between the monoclinic and tetragonal phases. When the ratio of the surface is higher than that of the bulk, the tetragonal phase is more favourable than the monoclinic phase. This implies that a smaller grain size, which has a larger surface ratio than larger grains, is favourable for inducing tetragonal-phase formation. The relative grain size, which is calculated from the full width at half maximum (FWHM) of the peak from (101) at 30.8°, indicates that the grain size decreases with increasing Y/Hf ratio, as shown in Fig. 2(b).

To characterise the chemical state of the films depending on the Y/Hf ratio, the binding energies of Y and Hf were investigated by means of XPS surface analysis. The peak position was recalibrated based on the C–C bond peak position (C1s peak), considering a binding energy of 285

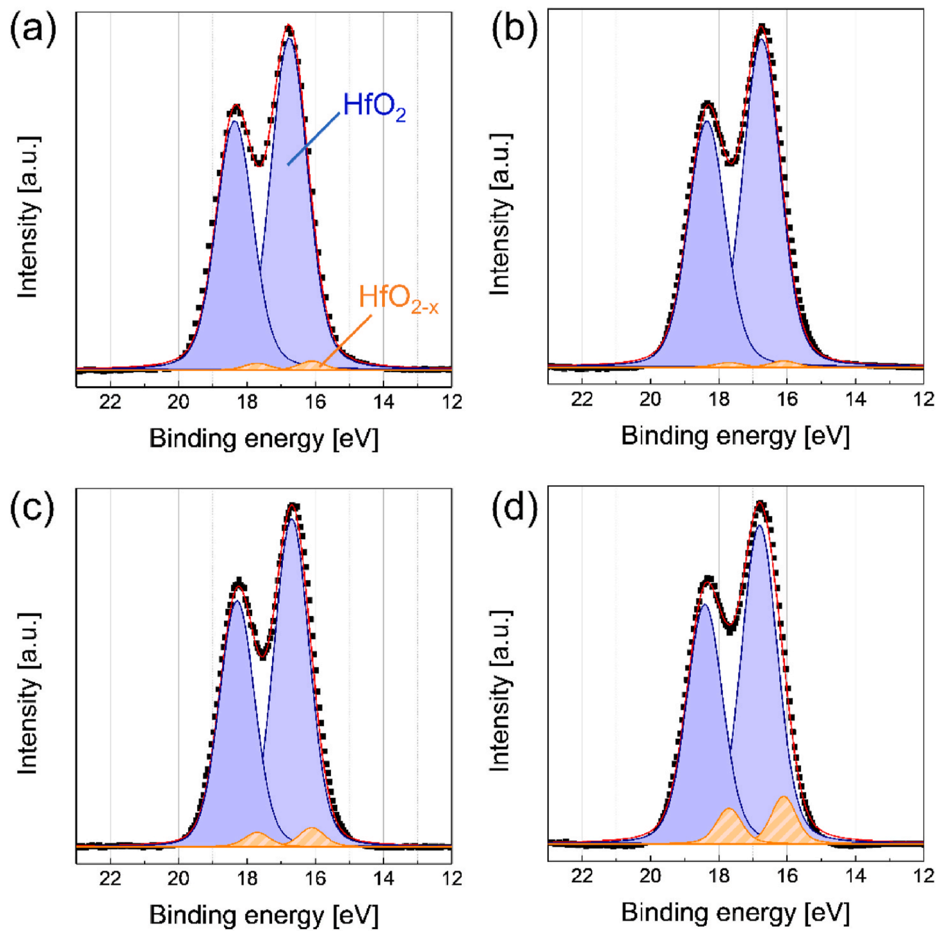

Fig. 4. Peak fits of Hf 4f of (a) HfO2, (b) YH-1, (c) YH-2, and (d) YH-3 thin films: in the Hf 4f spectra, the left-, and right-side peaks originated from $4f_{5/2}$, and $4f_{7/2}$, respectively. The peak deconvolution was conducted with $4f_{7/2}$ spectra (right-side peak).

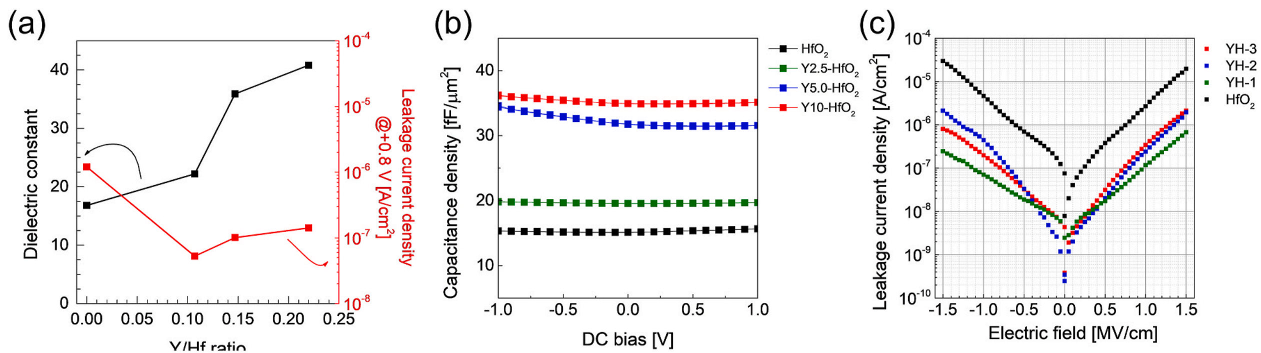

Fig. 5. (a) Dielectric constant (black, left axis) and leakage current density at an applied voltage of +0.8 V (red, right axis) versus Y/Hf ratio and (b) *C–V* curves, and (c) *J–E* curves of HfO_2, YH-1, YH-2, and YH-3 thin films with a thickness of 11 nm. (For interpretation of the references to colour in this figure legend, the reader is referred to the Web version of this article.)

eV. Fig. 3 shows the XPS profiles of the 3d core levels of Y for the Y-HfO_2 thin films. The Y 3d XPS profiles of the three samples are composed of Y $3d_{5/2}$ peaks centred at a binding energy of 179.8 eV with identical shapes, indicating that explain the Y dopant in the Y-HfO_2 thin film had identical chemical state regardless to the Y concentration in the cocktail precursor. In the case of the XPS profiles of the Hf 4f core levels, the spectrum was deconvoluted so that the Hf 4f peaks were composed of Hf $4f_{7/2}$ peaks centred at the 16.7- and 16.1-eV binding energies, which correspond to HfO_2 and HfO_{2-x} ($x < 1$), respectively (Fig. 4). The lower binding energy of the Hf 4f peak from HfO_{2-x} indicates that the Hf ion is less oxidised owing to the incorporation of V_O in the lattice. In this regard, there are two possible mechanisms for the formation of HfO_{2-x}: insufficient oxidation during the Y-HfO_2 thin-film deposition process and V_O formation by the incorporation of aliovalent Y_2O_3 into the HfO_2 lattice. The relative amounts of HfO_{2-x} to HfO_2 were 1.4, 1.0, 3.3, and 8.2 at.% for pristine HfO_2, YH-1, YH-2, and YH-3 thin films, respectively. The values of pristine HfO_2 and YH-1 thin films were almost identical, indicating that a small amount of Y dopant in HfO_2 does not induce significant V_O formation. Because the peak at a binding energy of 16.1 eV was significantly increased in the YH-2 and YH-3 thin films, the HfO_{2-x} formation is attributed to the formation of V_O by the incorporated Y dopant.

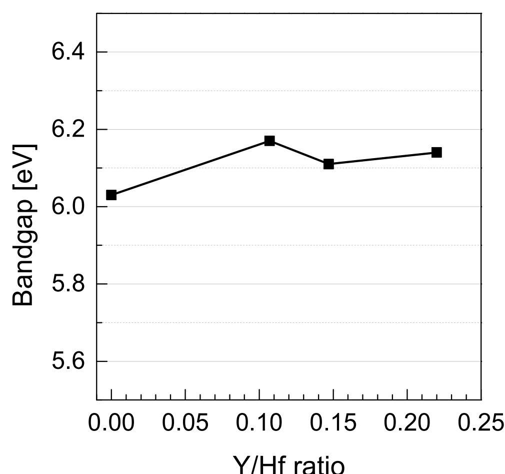

Fig. 6. Bandgap values of the insulators by the XPS analyses.

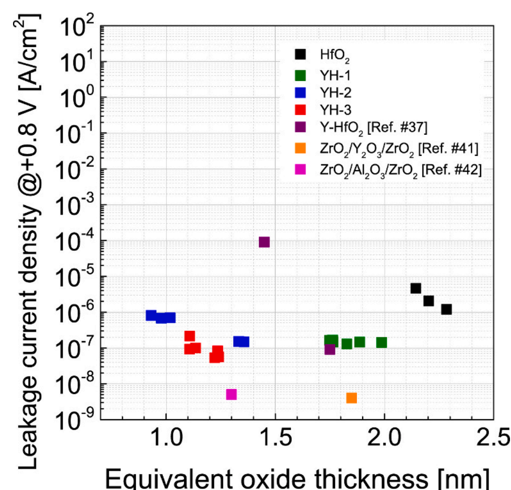

Fig. 8. J–t_{ox} plot of the MIM capacitor using HfO_2, YH-1, YH-2, and YH-3 thin films with a thickness of 10 nm.

The electrical property alteration of the HfO_2 thin film with respect to the tetragonal-phase transformation was evaluated. From the k value of 16.8 of the pristine HfO_2 thin film, the k values of the Y-HfO_2 thin film were increased to 22.2, 35.9, and 40.8 when the Y/Hf ratio was increased to 0.107, 0.147, and 0.220, respectively, as shown in Fig. 5(a). The k values were calculated from the capacitance density versus voltage (C–V) curve (Fig. 5(b)) of the MIM structures. The relationship between the k value and Y/Hf ratio implies that the tetragonal-phase transformation by the Y dopant effectively enhances the k value of the HfO_2 thin film. The relatively low k value (22.2) of the YH-1 thin film considering the crystal structure with only the tetragonal phase indicates that the Y dopant concentration of Y/Hf of 0.107 is not sufficient to induce complete crystallisation, but it is sufficient to suppress the monoclinic-phase formation. The k value of the YH-2 thin film revealed that complete crystallisation to the tetragonal phase is achieved when the Y/Hf ratio is 0.147 or higher. This was corroborated by the V_O ratio with respect to the Y/Hf ratio. Moreover, it should be emphasised that the significantly higher k values of 35.9 and 40.8 of the Y-HfO_2 thin film compared with the previous results could be achieved from a crystal structure consisting solely of the tetragonal phase. This enhancement was achieved by employing the cocktail precursor, which made possible the tetragonal-phase transformation to the entire region of the HfO_2 grain.

The leakage current density (J) of the Y-HfO_2 thin film was also improved compared with that of the pristine HfO_2 thin film by introducing the Y dopant. The pristine HfO_2 thin film exhibited a J value of 1.20×10^{-6} A/cm^2. The J value was significantly reduced to 5.27×10^{-8}, 1.01×10^{-7}, and 1.42×10^{-7} A/cm^2 for the YH-1, YH-2, and YH-3 thin films, respectively—see Fig. 5(a). As the leakage current density versus electric field (J–E) curves in Fig. 5(b) show, the J value difference between pristine HfO_2 and Y-HfO_2 thin films was observed in the entire examined electric-field region.

Electron conduction through the MIM structure employing HfO_2 as the insulator generally occurs with trap-assisted tunnelling and Poole–Frenkel emission [40,41]. Both conduction mechanisms are strongly related to the traps incorporated in the insulator. Indeed, the bandgap values of the insulators were almost identical (HfO2, YH-1, YH-2, and YH-3 of 6.03, 6.17, 6.11, and 6.14 eV, respectively, as shown in Fig. 6), implying that the conduction mechanism related to the barrier height, such as Schottky emission, was not affected by the J value difference. Moreover, because the bandgaps of the monoclinic and tetragonal phases are identical [42], the crystal structure difference between pristine HfO_2 and Y-HfO_2 does not induce the J value difference. Accordingly, it is inferred that V_O affects the leakage current property alteration in Y-HfO_2 thin films. Although it is well known that V_O increases J by contributing to trap-related carrier conduction, in the case of the Y-HfO_2 thin film, the J value was decreased compared with that of pristine HfO_2, even though the V_O concentration was increased by introducing the Y dopant, as shown in Fig. 4. The trap depth was calculated from the temperature-dependent J–E curve (Fig. 7). The trap depth decreased

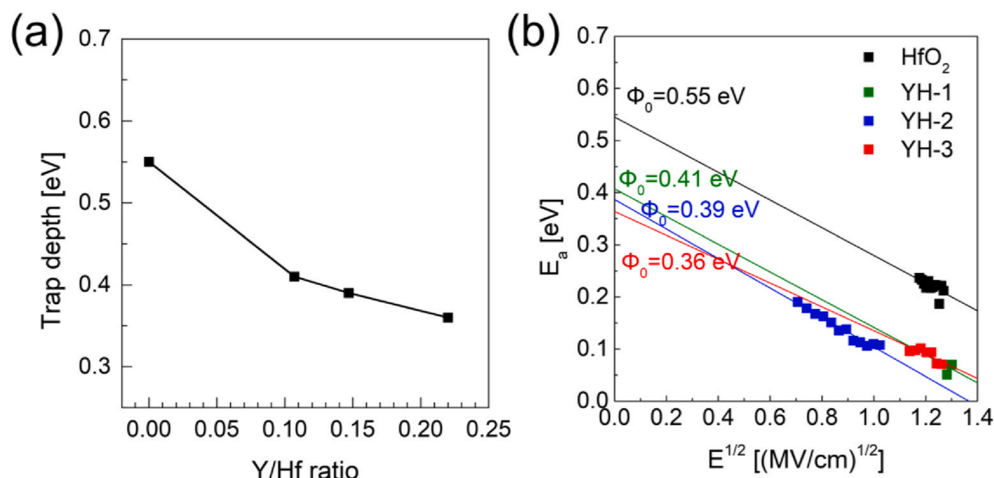

Fig. 7. (a) Calculated trap depth and (b) Ea versus $E^{1/2}$ plot from temperature-dependent J–E curves of HfO_2, YH-1, YH-2, and YH-3 thin films.

with Y doping, implying that V_O, which induces tetragonal-phase transformation, contributes to the formation of defect sites. The trap depth calculation also indicated that V_O defect formation from the Y dopant did not induce severe degradation of the *J* value. The mechanism of *J* property degradation by V_O in HfO_2 is the gap-state formation by the localised electrons at the neighbouring Hf ions from the V_O formation [43]. In other words, the defect site caused by V_O formation results from the partial occupation of Hf 5d orbitals by the electrons from V_O formation. However, V_O formation by the Y dopant does not accompany localised electron formation because it is related to the stoichiometry. Therefore, it can be postulated that V_O formation in HfO_2 by doping with an aliovalent dopant does not induce *J* property degradation.

Finally, the scaling of the equivalent oxide thickness (t_{ox}) was investigated using a J–t_{ox} plot (Fig. 8). By increasing the *k* value depending on the Y/Hf ratio, t_{ox} was decreased significantly from pristine HfO_2 of more than 2.0 nm to YH-2 and YH-3 of approximately 1.0 nm. This is significantly enhanced result compared with the previously reported results about ZrO_2- or HfO_2-based insulators [40,44]. Moreover, the *J* property was improved by increasing the Y/Hf ratio.

4. Conclusion

A Y-doped HfO_2 thin film using a Y + Hf cocktail precursor for DRAM capacitor dielectric applications was investigated. The Y-HfO_2 thin-film deposition process demonstrated homogeneous Y doping into the HfO_2 grain as a result of employing a cocktail precursor rather than the ALD supercycle process, resulting in a crystal structure consisting of the tetragonal phase with no contribution of the monoclinic phase. This crystal structure was induced by effective V_O formation in the HfO_2 grain from the ambivalent Y_2O_3, which stabilised the tetragonal phase of the HfO_2 thin film. Moreover, the change in grain size contributed to the tetragonal-phase transformation. Because of the tetragonal-phase formation, the *k* value of the HfO_2 thin film increased to 40.8 from 16.8 in the pristine HfO_2. The leakage current density was decreased by introducing the Y dopant simultaneously. Consequently, the performance of the MIM capacitor using the HfO_2-based insulator was significantly improved by adopting the Y + Hf cocktail precursor.

Author contributions

J. Kim, B. S. Kim, A. J. Lee, and D. H. Han performed thin film deposition, device fabrication, and characterization. J. H. Hwang, and Y. Kim carried out device fabrication. K.-C. Song, and H. Oh conducted synthesis of chemicals. S. Kim performed chemical analysis. Y. J. Park, and W. Jeon designed the experiment and co-wrote the paper. All of the authors discussed the results and commented on the paper.

Declaration of competing interest

The authors declare that they have no known competing financial interests or personal relationships that could have appeared to influence the work reported in this paper.

Acknowledgement

This work was supported by the Technology Innovation Program (No. 20003555, 20016813, and 20017216), and the Korea Institute of Energy Technology Evaluation and Planning (KETEP) grant (20201520300140, Development of Advanced Functional Material with C-14 from PHWR Waste) funded by the Ministry of Trade, Industry & Energy (MOTIE, Korea). W. Jeon also acknowledges financial support by SK Hynix.

References

[1] E.P. Gusev, C. Cabral, M. Copel, C. D'Emic, M. Gribelyuk, Ultrathin HfO2 films grown on silicon by atomic layer deposition for advanced gate dielectrics applications, Microelectron. Eng. 69 (2003) 145–151, https://doi.org/10.1016/S0167-9317(03)00291-0.
[2] J. Robertson, R.M. Wallace, High-K materials and metal gates for CMOS applications, Mater. Sci. Eng. R Rep. 88 (2015) 1–41, https://doi.org/10.1016/j.mser.2014.11.001.
[3] J. Robertson, New high-K materials for CMOS applications, Compr. Semicond. Sci. Technol. 1–6 (2011) 132–176, https://doi.org/10.1016/B978-0-44-453153-7.00120-6.
[4] C.H. Fu, K.S. Chang-Liao, C.C. Li, Z.H. Ye, F.M. Hsu, T.K. Wang, Y.J. Lee, M.J. Tsai, A higher-k tetragonal HfO 2 formed by chlorine plasma treatment at interfacial layer for metal-oxide-semiconductor devices, Appl. Phys. Lett. 101 (2012), https://doi.org/10.1063/1.4737393.
[5] Y. Lee, W. Jeon, Y. Cho, M.-H. Lee, S.-J. Jeong, J. Park, S. Park, x Al y Mesostructured Hf, O 2 thin films as reliable and robust gate dielectrics with tunable dielectric constants for high-performance graphene-based transistors, ACS Nano 10 (2016) 6659–6666, https://doi.org/10.1021/acsnano.6b01734.
[6] T.H. Perng, C.H. Chien, C.W. Chen, P. Lehnen, C.Y. Chang, High-density MIM capacitors with HfO2 dielectrics, Thin Solid Films (2004) 469–470, https://doi.org/10.1016/j.tsf.2004.08.148, 345–349.
[7] H. Hu, C. Zhu, Y.F. Lu, M.F. Li, B.J. Cho, W.K. Choi, A high performance MIM capacitor using HfO 2 dielectrics, IEEE Electron. Device Lett. 23 (2002) 514–516, https://doi.org/10.1109/LED.2002.802602.
[8] S.W. Jeong, H.J. Lee, K.S. Kim, M.T. You, Y. Roh, T. Noguchi, W. Xianyu, J. Jung, Effects of annealing temperature on the characteristics of ALD-deposited HfO2 in MIM capacitors, Thin Solid Films 515 (2006) 526–530, https://doi.org/10.1016/j.tsf.2005.12.288.
[9] P.K. Park, S.-W. Kang, Enhancement of dielectric constant in HfO[sub 2] thin films by the addition of Al[sub 2]O[sub 3], Appl, Phys. Lett. 89 (2006) 192905, https://doi.org/10.1063/1.2387126.
[10] A. Payne, O. Brewer, A. Leff, N.A. Strnad, J.L. Jones, B. Hanrahan, Dielectric, energy storage, and loss study of antiferroelectric-like Al-doped HfO2thin films, Appl. Phys. Lett. 117 (2020), https://doi.org/10.1063/5.0029706.
[11] Y.W. Yoo, W. Jeon, W. Lee, C.H. An, S.K. Kim, C.S. Hwang, Structure and electrical properties of Al-doped HfO2 and ZrO2 films grown via atomic layer deposition on Mo electrodes, ACS Appl. Mater. Interfaces 6 (2014) 22474–22482, https://doi.org/10.1021/am506525s.
[12] D.Y. Cho, H.S. Jung, I.H. Yu, J.H. Yoon, H.K. Kim, S.Y. Lee, S.H. Jeon, S. Han, J. H. Kim, T.J. Park, B.G. Park, C.S. Hwang, Stabilization of tetragonal HfO 2 under low active oxygen source environment in atomic layer deposition, Chem. Mater. 24 (2012) 3534–3543, https://doi.org/10.1021/cm3001199.
[13] G.R. Waetzig, S.W. Depner, H. Asayesh-Ardakani, N.D. Cultrara, R. Shahbazian-Yassar, S. Banerjee, Stabilizing metastable tetragonal HfO2 using a non-hydrolytic solution-phase route: ligand exchange as a means of controlling particle size, Chem. Sci. 7 (2016) 4930–4939, https://doi.org/10.1039/c6sc01601d.
[14] H. Kim, A. Marshall, P.C. McIntyre, K.C. Saraswat, Crystallization kinetics and microstructure-dependent leakage current behavior of ultrathin HfO 2 dielectrics: in situ annealing studies, Appl. Phys. Lett. 84 (2004) 2064–2066, https://doi.org/10.1063/1.1667621.
[15] C.-K. Lee, E. Cho, H.-S. Lee, C.S. Hwang, S. Han, First-principles study on doping and phase stability of HfO 2, Phys. Rev. B 78 (2008), 012102, https://doi.org/10.1103/PhysRevB.78.012102.
[16] M. Seo, S.K. Kim, J.H. Han, C.S. Hwang, Permittivity enhanced atomic layer deposited HfO2 thin films manipulated by a rutile TiO2 Interlayer, Chem. Mater. 22 (2010) 4419–4425, https://doi.org/10.1021/cm1010289.
[17] J.H. Lee, I.-H. Yu, S.Y. Lee, C.S. Hwang, Phase control of HfO2-based dielectric films for higher-k materials, J. Vac. Sci. Technol. B Microelectron. Nanom. Struct. 32 (2014), 03D109, https://doi.org/10.1116/1.4862952.
[18] R.C. Garvie, Stabilization of the tetragonal structure in zirconia microcrystals, J. Phys. Chem. 82 (1978) 218–224, https://doi.org/10.1021/j100491a016.
[19] C. Wang, M. Zinkevich, F. Aldinger, The Zirconia-Hafnia system: DTA measurements and thermodynamic calculations, J. Am. Ceram. Soc. 89 (2006) 3751–3758, https://doi.org/10.1111/j.1551-2916.2006.01286.x.
[20] M.W. Pitcher, S.V. Ushakov, A. Navrotsky, B.F. Woodfield, G. Li, J. Boerio-Goates, B.M. Tissue, Energy crossovers in nanocrystalline zirconia, J. Am. Ceram. Soc. 88 (2005) 160–167, https://doi.org/10.1111/j.1551-2916.2004.00031.x.
[21] A. Navrotsky, Thermochemical insights into refractory ceramic materials based on oxides with large tetravalent cations, J. Mater. Chem. 15 (2005) 1883–1890, https://doi.org/10.1039/b417143h.
[22] S.K. Kim, C.S. Hwang, Atomic layer deposition of ZrO2 thin films with high dielectric constant on TiN substrates, Electrochem. Solid State Lett. 11 (2008) G9, https://doi.org/10.1149/1.2825763.
[23] C. Viazzi, J.P. Bonino, F. Ansart, A. Barnabé, Structural study of metastable tetragonal YSZ powders produced via a sol-gel route, J. Alloys Compd. 452 (2008) 377–383, https://doi.org/10.1016/j.jallcom.2006.10.155.
[24] X. Huang, A. Zakurdaev, D. Wang, Microstructure and phase transformation of zirconia-based ternary oxides for thermal barrier coating applications, J. Mater. Sci. 43 (2008) 2631–2641, https://doi.org/10.1007/s10853-008-2480-x.
[25] X. Bokhimi, A. Morales, A. García-Ruiz, T.D. Xiao, H. Chen, P.R. Strutt, Transformation of yttrium-doped hydrated zirconium into tetragonal and cubic nanocrystalline zirconia, J. Solid State Chem. 142 (1999) 409–418, https://doi.org/10.1006/jssc.1998.8056.

[26] S.-M. Ho, On the structural chemistry of zirconium oxide, Mater. Sci. Eng. 54 (1982) 23–29, https://doi.org/10.1016/0025-5416(82)90026-X.

[27] T.S. Böscke, Crystalline Hafnia and Zirconia Based Dielectrics for Memory Applications Crystalline Hafnia and Zirconia based Dielectrics for Memory Applications Vom Promotionsausschuss der Doktor Ingenieur genehmigte Dissertation Berlin-Charlottenburg, 2018.

[28] J.E. Greedan, Introduction to the crystal chemistry of transition metal oxides, in: Handb. Solid State Chem., Wiley-VCH Verlag GmbH & Co. KGaA, Weinheim, Germany, 2017, pp. 161–220, https://doi.org/10.1002/9783527691036.hsscvol1005.

[29] J.S. Lee, W.H. Kim, I.K. Oh, M.K. Kim, G. Lee, C.W. Lee, J. Park, C. Lansalot-Matras, W. Noh, H. Kim, Atomic layer deposition of Y 2 O 3 and yttrium-doped HfO 2 using a newly synthesized Y(iPrCp) 2 (N-iPr-amd) precursor for a high permittivity gate dielectric, Appl. Surf. Sci. 297 (2014) 16–21, https://doi.org/10.1016/j.apsusc.2014.01.032.

[30] J. Niinistö, K. Kukli, T. Sajavaara, M. Ritala, M. Leskelä, L. Oberbeck, J. Sundqvist, U. Schröder, Atomic layer deposition of high-permittivity Yttrium-doped Hf O2 films, Electrochem. Solid State Lett. 12 (2008) 12–15, https://doi.org/10.1149/1.3020763.

[31] P.D. Lomenzo, Q. Takmeel, C. Zhou, C.C. Chung, S. Moghaddam, J.L. Jones, T. Nishida, Mixed Al and Si doping in ferroelectric HfO2 thin films, Appl. Phys. Lett. 107 (2015), https://doi.org/10.1063/1.4937588.

[32] W. Jeon, S.H. Rha, W. Lee, Y.W. Yoo, C.H. An, K.H. Jung, S.K. Kim, C.S. Hwang, Controlling the Al-doping profile and accompanying electrical properties of rutile-phased TiO 2 thin films, ACS Appl. Mater. Interfaces 6 (2014) 7910–7917, https://doi.org/10.1021/am501247u.

[33] K. Kukli, J. Niinistö, A. Tamm, J. Lu, M. Ritala, M. Leskelä, M. Putkonen, L. Niinistö, F. Song, P. Williams, P.N. Heys, Atomic layer deposition of ZrO2 and HfO2 on deep trenched and planar silicon, Microelectron. Eng. 84 (2007) 2010–2013, https://doi.org/10.1016/j.mee.2007.04.035.

[34] X. Tian, S. Shibayama, T. Nishimura, T. Yajima, S. Migita, A. Toriumi, Evolution of ferroelectric HfO2 in ultrathin region down to 3 nm, Appl. Phys. Lett. 112 (2018), https://doi.org/10.1063/1.5017094, 0–5.

[35] Y. Zhang, J. Xu, C.K. Choi, Z.X. Fang, P. Li, L. Yuan, L. Chen, Investigation of temperature-dependent ferroelectric properties of Y-doped HfO2 thin film prepared by medium-frequency reactive magnetron co-sputtering, Vacuum 179 (2020) 109506, https://doi.org/10.1016/j.vacuum.2020.109506.

[36] A. Tamm, K. Kukli, J. Niinistö, J. Lu, M. Ritala, M. Leskelä, Properties of HfO 2 and HfO 2 : Y films grown by atomic layer deposition in an advanced monocyclopentadienyl-based process, IOP Conf. Ser. Mater. Sci. Eng. 8 (2010), 012022, https://doi.org/10.1088/1757-899x/8/1/012022.

[37] J. Niinistö, M. Mäntymäki, K. Kukli, L. Costelle, E. Puukilainen, M. Ritala, M. Leskelä, Growth and phase stabilization of HfO2 thin films by ALD using novel precursors, J. Cryst. Growth 312 (2010) 245–249, https://doi.org/10.1016/j.jcrysgro.2009.10.028.

[38] W. Zhang, G. Li, X. Long, L. Cui, M. Tang, Y. Xiao, S. Yan, Y. Li, W. Zhao, A comparative study of the γ-ray radiation effect on Zr-doped and Al-doped HfO2-based ferroelectric memory, Phys. Status Solidi Basic Res. 257 (2020) 2–7, https://doi.org/10.1002/pssb.201900736.

[39] G. Witz, V. Shklover, W. Steurer, S. Bachegowda, H.P. Bossmann, Phase evolution in yttria-stabilized zirconia thermal barrier coatings studied by rietveld refinement of X-ray powder diffraction patterns, J. Am. Ceram. Soc. 90 (2007) 2935–2940, https://doi.org/10.1111/j.1551-2916.2007.01785.x.

[40] W. Jeon, O. Salicio, A. Chaker, P. Gonon, C. Vallee, Controlling the current conduction asymmetry of HfO 2 metal–insulator–metal diodes by interposing Al 2 O 3 layer, IEEE Trans. Electron. Dev. 66 (2019) 402–406, https://doi.org/10.1109/TED.2018.2881220.

[41] W. Jeon, Recent advances in the understanding of high-k dielectric materials deposited by atomic layer deposition for dynamic random-access memory capacitor applications, J. Mater. Res. 35 (2020) 775–794, https://doi.org/10.1557/jmr.2019.335.

[42] H. Jiang, R.I. Gomez-Abal, P. Rinke, M. Scheffler, Electronic band structure of zirconia and hafnia polymorphs from the GW perspective, Phys. Rev. B Condens. Matter 81 (2010) 1–9, https://doi.org/10.1103/PhysRevB.81.085119.

[43] M.V. Ganduglia-Pirovano, A. Hofmann, J. Sauer, Oxygen vacancies in transition metal and rare earth oxides: current state of understanding and remaining challenges, Surf. Sci. Rep. 62 (2007) 219–270, https://doi.org/10.1016/j.surfrep.2007.03.002.

[44] C.H. An, W. Lee, S.H. Kim, C.J. Cho, D.-G. Kim, D.S. Kwon, S.T. Cho, S.H. Cha, J. I. Lim, W. Jeon, C.S. Hwang, Controlling the electrical characteristics of ZrO 2/Al 2</inf> O 3/ZrO 2 capacitors by adopting a Ru top electrode grown via atomic layer deposition, Phys. Status Solidi Rapid Res. Lett. $_{13}$ (2019), https://doi.org/10.1002/pssr.201800454.